Clinical Neurophysiology 128 (2017) 1696–1706

Contents lists available at ScienceDirect

Clinical Neurophysiology

journal homepage: www.elsevier.com/locate/clinph

Stereo-electroencephalography identifies N2 sleep and spindles in human hippocampus

Nicolas Carpentier [a,*], Thierry Cecchin [b,c], Laurent Koessler [b,c], Valérie Louis-Dorr [b,c], Jacques Jonas [a,b,c], Jean-Pierre Vignal [a,b,c], Marc Carpentier [d], William Szurhaj [e], Patrice Bourgin [f], Louis Maillard [a,b,c]

[a] Department of Neurology, Nancy University Hospital, Nancy, France
[b] CNRS, CRAN, UMR 7039, Nancy, France
[c] Université de Lorraine, CRAN, UMR 7039, Nancy, France
[d] Division of Clinical Epidemiology, Geneva University Hospitals, Geneva, Switzerland
[e] Department of Neurology, Salengro University Hospital, Lille, France
[f] Sleep Disorder Center and CNRS UPR3212, Strasbourg University Hospital, Strasbourg, France

ARTICLE INFO

Article history:
Accepted 15 June 2017
Available online 8 July 2017

Keywords:
Hippocampus
Sleep
Stereo-electroencephalogram
Stereo-electroencephalography
Spindles
N2 sleep
Intracerebral recording
Depth recording

HIGHLIGHTS

- The absolute powers of the hippocampal signal are distinct during N2 stage compared to N3 stage.
- The hippocampal sleep spindles exhibit a frequency closer to fast than slow cortical spindles.
- The analysis of sleep cycles suggests a homeostatic process within hippocampus.

ABSTRACT

Objectives: To describe the hippocampal stereo-electroencephalogram during sleep according to sleep stages (including N2 sleep) and cycles, together with the hippocampal spindles.
Methods: All patients with drug-resistant focal epilepsy undergoing intra-hippocampal implantation between August 2012 and June 2013 at Nancy University Hospital were screened. Six patients with explored hippocampus devoid of pathological features were analyzed. During one night, we identified continuous periods of successive N2, N3 and REM sleep for two full cycles. We performed a spectral analysis of the hippocampal signal for each labeled sleep period.
Results: N2, N3 and REM sleeps were individualized according to their spectral powers, for each frequency band and sleep cycle. Hippocampal spindles showed dynamic intrinsic properties, the 11.5–16 Hz frequency band being mainly dominant, whereas the 9–11.5 Hz frequency band heightening during the beginning and the end of the transient. For N3 and REM sleep stages, the power of the hippocampal signal was significantly decreased between the first and the second sleep cycle.
Conclusion: Distinct N2 sleep, fast spindles and homeostatic profile are all common properties shared by hippocampus and cortex during sleep.
Significance: The close functional link between hippocampus and cortex may have various sleep-related substrates.

1. Introduction

Physiological activity and related functions of the hippocampus are clearly modulated by sleep. For example, the sequences of hippocampal neuronal discharges in rats occurring during a space exploration are reactivated during both non-rapid eye movement (NREM) and rapid eye movement (REM) sleep (Wilson and McNaughton, 1994; O'Neill et al., 2008). In humans, this so-called hippocampal replay was also highlighted in positron emission tomography (PET) in healthy volunteers during slow-wave sleep (SWS) the night following a mnesic episodic learning task (Peigneux et al., 2004).

* Corresponding author at: Centre Hospitalier Universitaire de Nancy, Hôpital Central, Service de Neurologie, 29 avenue du Maréchal de Lattre de Tassigny, Nancy F-54000, France.
E-mail address: n.carpentier@chru-nancy.fr (N. Carpentier).

http://dx.doi.org/10.1016/j.clinph.2017.06.248
1388-2457/

Intracerebral recordings (Stereo-electroencephalogram) performed during pre-surgical work-up in patients with refractory epilepsy have allowed for description of several hippocampal electrophysiological patterns associated with either NREM or REM sleep. For example, ripples and fast ripples were detected in significantly greater quantities during SWS than in REM sleep (Staba et al., 2004; Skaggs et al., 2007). Hippocampal sharp-waves (SPW) have been found to occur mainly during NREM sleep, since more than 80% of the ripples were found to be associated with hippocampal SPW during SWS (Urrestarazu et al., 2007). Sleep spindles were observed in hippocampus during NREM sleep (Andrillon et al., 2011; Nir et al., 2011), but also before sleep onset (Sarasso et al., 2014), and were modulated by interictal hippocampal spiking (Frauscher et al., 2015). Interestingly, both hippocampal SPW and spindles have been linked to memory consolidation (Jadhav et al., 2012; Genzel et al., 2014).

Intracerebral studies have brought various but sometimes inconsistent results about hippocampal REM sleep. By using stereo-electroencephalography (SEEG), Cantero and coworkers reported short bursts of theta (4–7 Hz) oscillations (Cantero et al., 2003), whereas Moroni et al. found high delta (2–4 Hz) oscillations during both REM sleep and wakefulness (Moroni et al., 2012). Other studies based on juxta-hippocampal electrocorticography (ECoG), reported slower (1.5–3 Hz) oscillations during REM sleep (Bódizs et al., 2001; Clemens et al., 2009). Moroni and coworkers, while still keeping this NREM-REM sleep dichotomy, proposed a time–frequency-based descriptive analysis of a wide frequency spectrum divided into so-called "physiological" bands (Moroni et al., 2007). This method offers the advantage of clarifying the everyday SEEG visual analysis based on global changes of power of the hippocampal SEEG signal observed in the major physiological frequency bands during the successive NREM-REM cycles. Overall, the signal power was found to be lower during REM sleep compared to NREM sleep for all studied frequency bands, with a lower relative decrease in the very low frequency band (VLF: 0.5–1 Hz) and beta frequency band (15.1–30 Hz).

The use of SEEG is being expanding a lot in surgical epilepsy centers. We need to identify exhaustively physiological patterns of hippocampal signal to address research issues like sleep effect on hippocampal functions. Surprisingly, none of the previous studies differentiated hippocampal N2 from N3 sleep, two sleep stages characterized by very different electrophysiological features, like the sleep spindles that are known to mainly occur during N2 sleep in cortical areas. In this context, the purpose of our work was to provide a further comprehensive description of the human hippocampal electrophysiological activity specifically during N2 sleep. We first performed a time–frequency-based analysis to compare the main frequency bands of hippocampal signal according to N2, N3, REM stages and sleep cycles. Second, we analyzed the intrinsic variables of the hippocampal spindles to determine their duration, amplitude, and main frequencies.

2. Materials and methods

2.1. Patients

From August 2012 to June 2013, 10 of the 15 patients undergoing SEEG for drug-resistant focal epilepsy in the Nancy University Hospital were consecutively included according to the following criteria: at least one explored hippocampus (i) without any structural abnormality in magnetic resonance imaging (MRI), and (ii) without any ipsilateral metabolic abnormalities identified by PET with fluorine-18 fluorodeoxy-glucose ([^{18}F]FDG). The goal of the SEEG was to estimate the epileptogenic zone (EZ) to propose a potential curative surgical resection. Six patients (including 2 patients with bilateral hippocampal implantation) were finally analyzed as they met the following criteria: (i) EZ sparing the ipsilateral hippocampus, (ii) no disturbed background activity of ipsilateral hippocampal SEEG signal, (iii) rare or no ipsilateral hippocampal interictal epileptiform activity, (iv) at least 2 full sleep cycles, and (v) absence of any comorbid sleep disorders as assessed by a systematic structured screening (narcolepsy with or without cataplexy, sleep apnea, restless legs syndrome, chronic severe insomnia, severe psychiatric disorder). All patients gave their written informed consent to participate to the study. Six hippocampi (left-sided: 3) were finally analyzed, belonging to six different patients (male: 3, median age: 32.5 years, age range: 23–37 years). The clinical characteristics of the patients and their medications are reported in Table 1. None had an associated sleep disorder.

2.2. Procedure of SEEG and polygraphic video recordings

2.2.1. SEEG video recordings

The intracerebral electrodes were composed of 5–18 circular contacts, each with a diameter of 0.8 mm, a contact length of 2.0 mm and an intercontact distance of 1.5 mm (Medical Dixi©, Besançon, France). The procedure of stereotactic placement of the intracerebral electrodes was described in a previous paper by our group (Jonas et al., 2015). Each patient had at least one contact located unambiguously in the anterior part of area 1 of cornu ammonis (CA1) of the hippocampus (Fig. 1). The reference electrode was a cup-shaped surface electrode (Impedance <5 kΩ), placed in FPz position according to the international 10/20 system. The SEEG signal was recorded on a 128-channel amplifier at a 512 Hz sampling rate (2 SD LTM 64 Headbox©, Micromed, Italy; analog high-pass filter: 0.5 Hz; analog low-pass filter: 1800 Hz; digital low-pass filter: 231.5 Hz; precision conversion: 22 bits). A high-definition video coupled with an infrared video for low luminosity was synchronized with the SEEG signal to carry out 24 h/day time-locked electro-clinical correlations. The SEEG data were stored on a SEEG server through SystemPlus Evolution© software (Micromed, Italy). Acquisition files were converted to ASCII files to be handled with MatLab© software (MatLab 7.0, The Matworks, Inc.).

2.2.2. Polygraphic video recordings

Seven surface electrodes recorded the EEG: C3, C4, O1, O2, T3, T4 and Fz as the reference (10/20 system, impedance <5 kΩ). Two bipolar electrodes, respectively placed 1 cm below the left outer canthus (EOG 1), and 1 cm above the right outer canthus (EOG 2), recorded the electrooculogram (EOG). Two chin bipolar electrodes recorded the electromyogram (EMG). The EEG, EOG and EMG surface signal was recorded on an ambulatory polygraph device at a 256 Hz sampling rate (Morpheus©, Micromed, Italy). The intracerebral implantation was performed on day 1 and the simultaneous SEEG/polygraphic video recordings occurred the night following day 2. We tested each channel individually for impedance, and quality of the signals before recordings. The polygraph was time-synchronized with the SEEG video acquisition platform on day 2 at 09:00 PM. Then patients switched the light off as they wished. The following morning on day 3, the polygraph was shut off at 06:00 AM and SEEG and polygraphic data were transferred to the storage server.

2.3. Visual analysis of polygraphic and SEEG video recordings

2.3.1. Polygraphic video recordings

Sleep was scored in 30 s epochs according to the 2007 criteria of the American Academy of Sleep Medicine (Iber, 2007). For each sleep stage (N2, N3 and REM), we selected the longest period of

Table 1
Clinical data of the six analyzed patients.

Patient	Sex	Age (y)	AED	mg/day	AD	Contact	EZ
1	M	32	Carbamazepine	200	Propofol	B′3	T[a]
			Lincosamide	200	Remifentanil	B′4	
			Pregabalin	100	Paracetamol	B′5	
			Lamotrigine	100	Nefopam		
					Hydroxyzine		
2	F	36	Eslicarbazepine	0	Propofol	B′1	STG
					Remifentanil	B′2	
					Paracetamol	B′3	
					Morphine	B′4	
					Droperidol	B′5	
3	F	37	Lamotrigine	250	Propofol	B1	O
			Pregabalin	50	Remifentanil	B2	
			Escitalopram	15	Paracetamol	B3	
					Nefopam		
4	F	29	Levetiracetam	1000	Propofol	B′1	TPj
			Phenobarbital	100	Remifentanil	B′2	
					Paracetamol	B′3	
					Nefopam	B′4	
					Domperidone		
5	M	33	Oxcarbazepine	1200	Propofol	B2	T[a]
			Pregabalin	0	Remifentanil	B3	
					Paracetamol	B4	
						B5	
6	M	23	Eslicarbazepine	600	Propofol	B1	T[a]
			Lincosamide	400	Remifentanil	B2	
			Clobazam	15	Paracetamol	B3	
					Nefopam	B4	
						B5	

F: Female; M: Male; y: years; AED: Antiepileptic drugs during the recorded night; AD: Anesthetic drugs during surgery the day before; EZ: Epileptogenic zone; T: Temporal; O: Occipital; STG: Superior temporal gyrus; TPj: Temporo-parietal junction.
[a] Contra-lateral to the analyzed contacts.

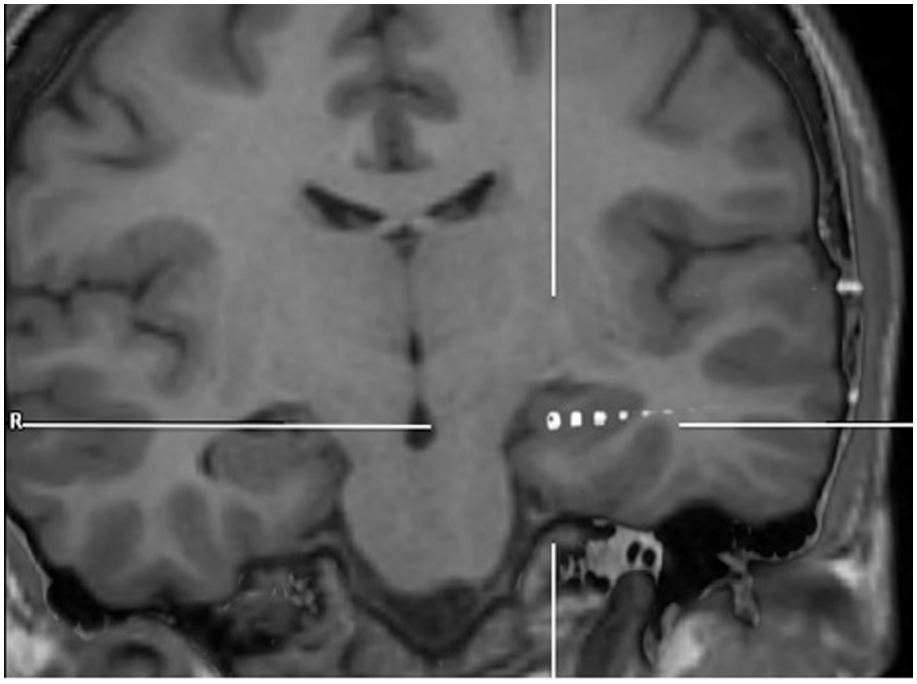

Fig. 1. Localization of the medial contacts of the left (') hippocampal (B) electrode of patient 2, by a MRI 3D T1 coronal slice. The white cross-bars target the contact B′ n° 1, within the gyrus dentatus. Contact B′ n° 4 was unambiguously located in area 1 of cornu ammonis (CA1) of the left hippocampus and was thus selected for the analysis.

continuous and uninterrupted sleep. The selected sleep segments were coded with the corresponding cycle and the corresponding stage defining the hierarchical structure of sleep (e.g.: C2N3 was used to code the segment of N3 sleep stage from the second sleep cycle C2). Only two sleep cycles with subsequent N2, N3 and REM stages ("full" sleep cycles) were available for all the patients. For each patient, the duration of the selected segments according to the sleep stages are reported in Table S1. The selected segments showed unequal durations between stages and patients due to noticeable variability of sleep quality.

2.3.2. SEEG video recordings

The first step was the delineation of the EZ, based on the visual analysis of the 24 h/day SEEG video recordings. All traces were visually analyzed by experienced epileptologists (LM, JPV). The EZ was delineated by the contacts recording the earliest rhythmic low voltage fast activity or rhythmic discharges, at the onset of spontaneous seizures (Kahane et al., 2006). Two additional hippocampi outside of the EZ were excluded from the analysis based on the presence of abundant inter-ictal epileptiform activity (each one coming from the 2 patients with bilateral hippocampal implantation). For the remaining six recorded hippocampi, only segments of sleep without any epileptic spikes were finally selected for the analysis. Representative samples of N2, N3 and REM sleep are shown in Fig. 2.

2.4. Analysis of hippocampal signal powers according to sleep stages and cycles

Only the SEEG monopolar signal of the selected segments from the contact most strictly located within the CA1 of the hippocampus was analyzed. A time–frequency analysis of the absolute energy was performed based on dyadic-type wavelet decomposition with a sliding window of 5 s. The frequencies were grouped into the four following bands: delta (0.5–4 Hz), theta (4–8 Hz), alpha (8–13 Hz) and beta (13–30 Hz). For all the patients and for all the selected sleep segments, a set of values of the absolute power was obtained. To compare data between patients, we normalized the absolute powers from the four specified frequency bands by the total power. To study how the normalized power of the recorded signal was associated with frequency bands, cycles and stages, we used a mixed model. This allowed accounting for both the unbalanced dataset (available data differs between cycles and stages, and from one patient to another because of different durations of the selected segments and their subsets of cycles/stages) and their hierarchical structure (powers in each bandwidth belong to some sampling time; and measures belong to some patient). The outcome was the logarithm of the power; effects are therefore expressed as ratios between bands, cycles or stages (after exponienting the estimated coefficients). The hierarchical structure of data was specified with a nested random effect on the intercept, with measures (defined as the simultaneous measurement of the powers in the four frequency bands of interest) nested in patients. Our questions were studied with fixed effects for frequency bands, cycles and stages; and two-way interactions between these variables (cycle-stage, stage-band, cycle-band). Only the significant interactions were kept for the final model. The global significance of the different variables and interactions were tested with a 5% α cut-off. Due to interactions, effects for the cycles and effects for the stages were expressed by calculating the appropriate contrasts. For each contrast of the considered effects (cycle effects and stage effects), a Bonferroni correction was used to assess the significance of the effects and to compute their confidence intervals. Statistical analyzes were performed with the version 3.0.2 of R CRAN© software (R-Core-Team, 2013).

2.5. Detection of hippocampal sleep spindles

Similarly, only the SEEG monopolar signal of the selected segments from the contact most strictly located within the CA1 of the hippocampus was analyzed. The identification of spindles proceeded in two steps: first an automatic detection of potential spindles and secondly a visual validation by the expert. For the automatic detection of potential spindles, the monopolar signal was first band-pass filtered (8.5–16.5 Hz, −0.1 dB at 9 Hz and 16 Hz) using a Hamming window-based Finite Impulse Response (FIR) filter (n = 1000). These cut-off frequency values were chosen to detect slow (9–12 Hz) and fast (13–15 Hz) spindles according to Andrillon et al. (2011). Then the instantaneous amplitude of the obtained signal was computed via the Hilbert transform and smoothed with a low-pass FIR filter (5 Hz, n = 200). This amplitude was compared to a threshold and, if the period during which the signal exceeded the threshold was greater than 0.5 s, the detected event was considered as a potential spindle. To take into account the variability of background activity across subjects, the threshold amplitude was set at 2 standard deviations (SD) of the band-pass filtered signal, computed on the whole segment. The value of both the low-pass filter cut-off frequency and the threshold were adjusted after testing with short segments of signal containing validated spindles. The time period was a priori set considering that the minimum spindle duration was 0.5 s. After this step of automatic detection, all the potential detected spindles were visually validated (NC) from the raw signal and the beginning and the end of the validated spindles were visually marked. Then these marks were precisely adjusted at the nearest negative extreme from the band-pass filtered signal.

2.6. Description of hippocampal spindles

Preliminary, a visual analysis of the filtered signal and of the corresponding FFT of each validated spindle indicated that a spindle could be mainly modeled by one or two sinusoids with modulated amplitude. Then, for each spindle, the duration and the mean amplitude were computed, and the frequency spectrum was estimated using the Yule-Walker autoregressive (AR) method of spectral estimation (model order: 60, spectral accuracy: 0.25 Hz; the model order was selected to obtain a smoothed spectrum with a clear visualization of the main frequencies) (Kay, 1988). This method allowed identifying the two main frequencies of the spindle. The mean of these characteristics were computed globally and for each patient. The two-sample Kolmogorov-Smirnov test was used to determinate whether the repartition of the main frequencies in the window (9–16 Hz) reflects a continuous distribution or two distinct sets of data. (This nonparametric hypothesis test evaluates the difference between the cumulative distribution functions of the distributions of the two data sets over the range of x in each data set. It uses the maximum absolute difference between the cumulative distribution functions. The test statistic is: $D = \max_x\left(\left|\widehat{F}_1(x) - \widehat{F}_2(x)\right|\right)$ where $\widehat{F}_1(x)$ is the proportion of x_1 values less than or equal to x and $\widehat{F}_2(x)$ is the proportion of x_2 values less than or equal to x). To further investigate the characteristics of the spindles, we first studied the static relationship between their main frequency and amplitude and between the two main frequencies if present. Afterwards, we studied their dynamical properties. We (i) performed a time–frequency analysis of the filtered spindles (a short-time Fourier transform associated with a Hamming window was used, the signal was divided into 20 segments with 80% overlapping samples to obtain a time–frequency resolution tradeoff; these settings, combined with a shading of the obtained surface, gave a smoothed spectrogram) and (ii) assessed the time course of the dominant frequency within the spindles by using the second Hjorth descriptor called mobility (Hjorth, 1973). An exponential moving average with a weighting factor equal to 0.08 was used and the obtained mobility was smoothed with a low-pass FIR filter (16 Hz, n = 70). With these settings, obtained after testing with validated spindles, the initialization window was about 50 samples (i.e. about 100 ms). Depending on the observed trends of the mobilities, we focused on time intervals of interest within the spindles by removing samples from the beginning or the end of the transient. Consequently, we updated the corresponding intrinsic characteristics of the spindles. We used appropriate tests of proportions comparison with adequate Bonfer-

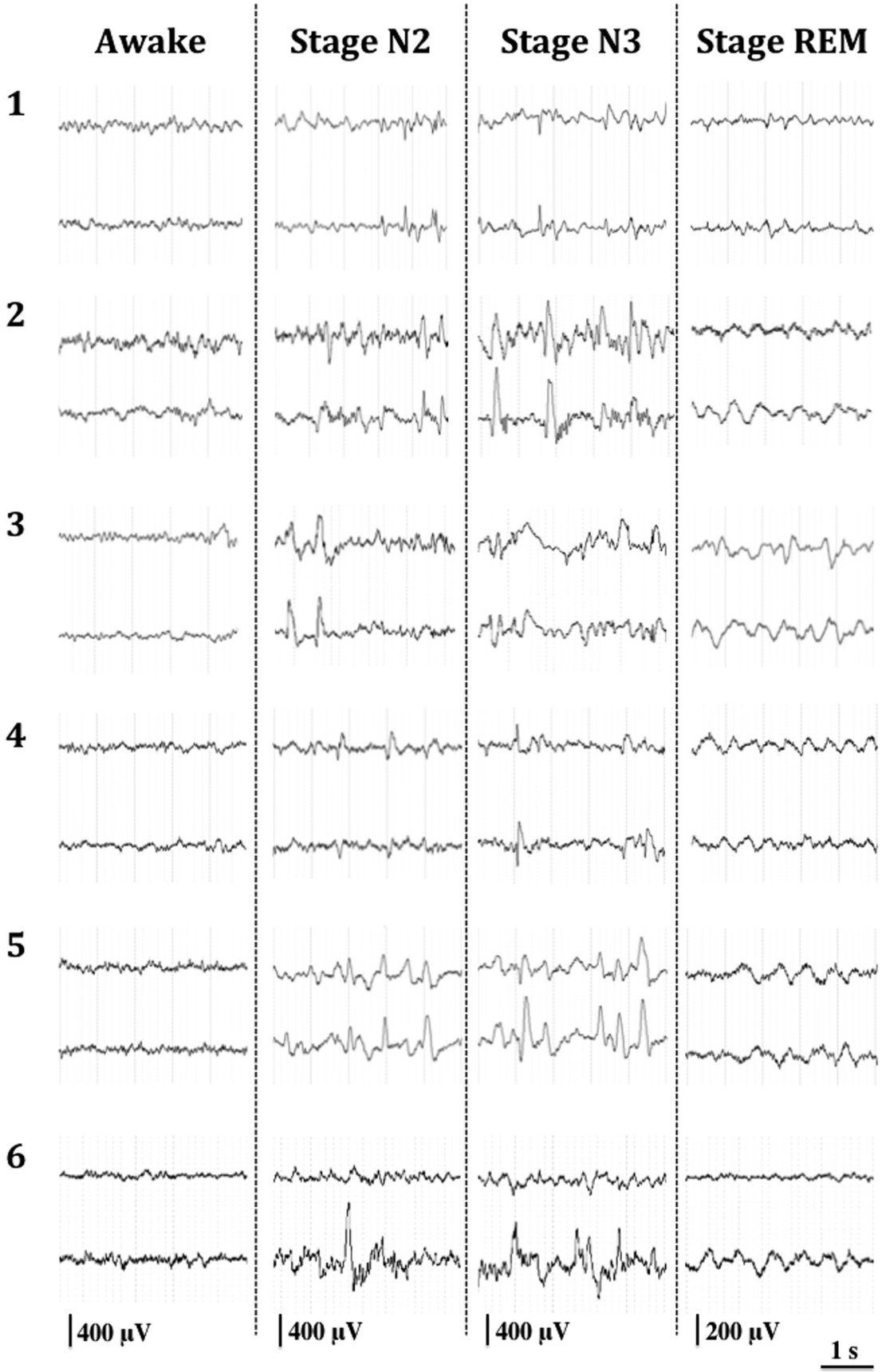

Fig. 2. Overview of the hippocampal background activity awake and across the sleep stages. For the six analyzed patients (number), four samples of five seconds from hippocampal recordings are shown: each one successively refers to awake state, N2, N3 and REM (Rapid-eye-movement) sleep. For each patient, the two channels come from a bipolar montage, linking the contact located within CA1 with the adjacent medial (upper channel) and adjacent lateral contact (lower channel).

roni corrections to assess the effect of adjusting the beginning and the end of the spindles both on the repartition of the main frequencies and on the proportion of single-frequency spindles. (Let p_1 and p_2 the two proportions to compare, estimated from two samples of size n_1 and n_2, the test statistic is: $u = \frac{p_1 - p_2}{\sqrt{p(1-p)\left(\frac{1}{n_1}+\frac{1}{n_2}\right)}}$ with: $P = \frac{n_1 p_1 + n_2 p_2}{n_1 + n_2}$. Under H_0 hypothesis, that is $p_1 = p_2$, the test statistic would be from a standard normal distribution).

3. Results

3.1. Descriptive statistics and comparison of powers between sleep segments

The mean absolute powers of the different sleep segments according to the four frequency bands are represented in Fig. S1. Concerning the comparative analysis, for the two full sleep cycles, there were statistically significant interactions between the effects of cycles and stages ($p < 0.01$), and between the effects of stages and frequency bands ($p < 0.01$). The contrasts in power between N2 and N3 (N3/N2 ratios) were calculated for each combination of cycle and frequency band. In the same way, REM/N2 ratios and REM/N3 ratios were calculated. These effects are summarized in Table S2, and presented in subplot A of Fig. 3. N3/N2 ratios were significantly superior to 1 for the delta band during C1 and C2. For theta, alpha and beta bands, N3/N2 ratios were significantly superior to 1 during C1, whereas during C2, N3/N2 ratios for theta (not significant), alpha and beta bands were inferior to 1. REM/N2 ratio was superior to 1 for the delta band during C1 (without statistical significance). On the contrary, REM/N2 ratios were significantly inferior to 1 for the delta band during C2. For theta, alpha and beta bands, REM/N2 ratios were significantly inferior to 1 during C1 and C2. REM/N3 ratios were significantly inferior to 1 for all the fre-

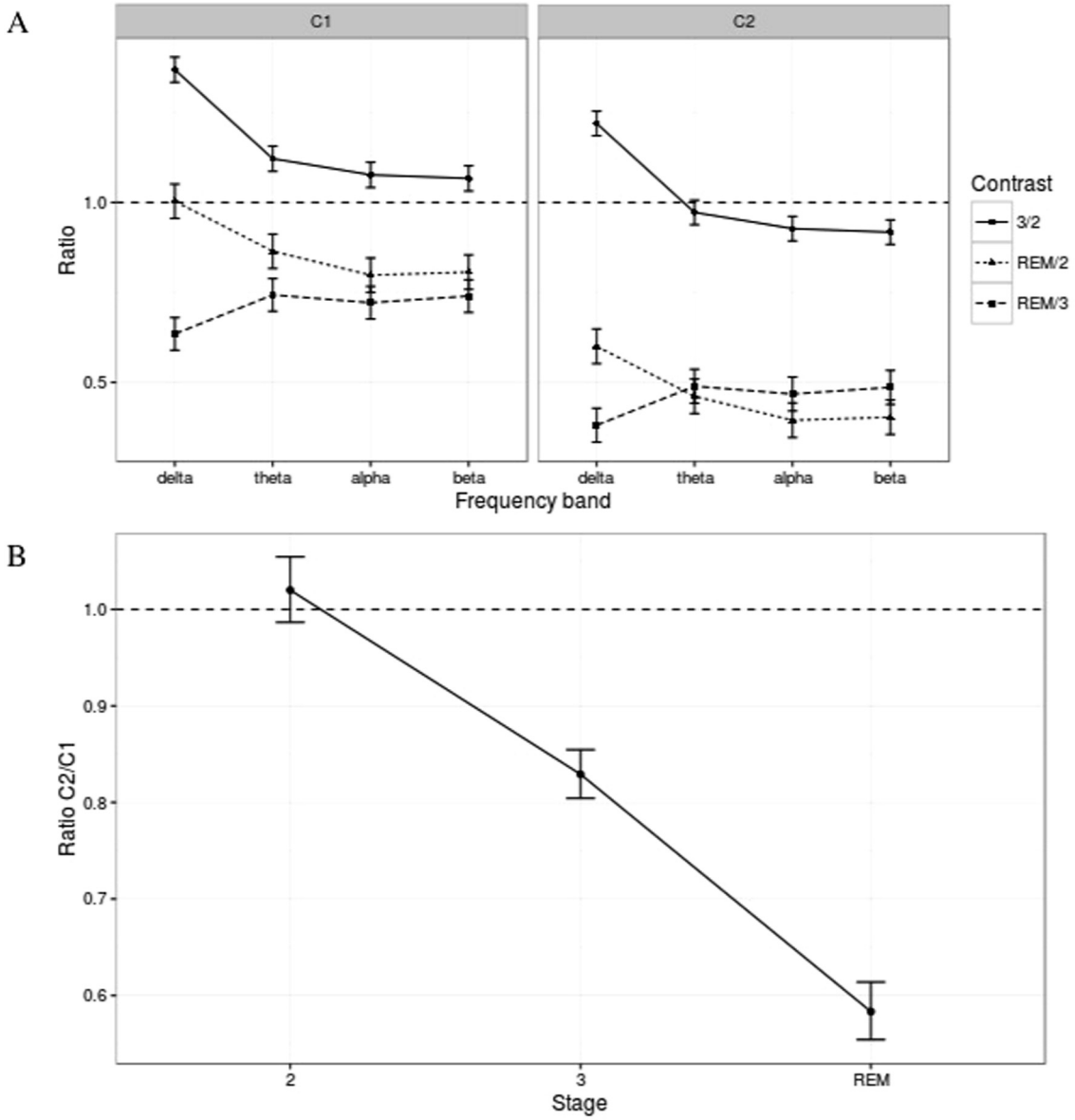

Fig. 3. Contrasts between sleep stages and between sleep cycles. Error bars show the estimated confidence intervals. (A) Contrasts between sleep stages. Effects were assessed by pairwise comparisons between stages. Because of the interactions between the effects of cycles and stages and between the effects of stages and frequency bands, the contrasts for the effects of stages are expressed for the four frequency bands (abscissa) and for cycle 1 and cycle 2 (respectively the left and right frames). (B) Contrasts between sleep cycles. Effects were assessed by a pairwise comparison between cycles (C2/C1). Because of the interaction between the effects of cycles and stages, the C2/C1 ratios are expressed for N2, N3 and REM sleep.

Table 2
Summary of the contrasts between sleep cycles.

Stage	C2/C1 Ratio	Lower limit	Upper limit	*P* value
N2	1.02	0.98	1.06	0.245
N3	0.83	0.80	0.86	<0.001*
REM	0.58	0.55	0.62	<0.001*

Effects were assessed by pairwise comparisons between sleep cycles (C1, C2). For each stage, the value of the C2/C1 ratio is presented with lower and upper limits of its confidence interval, estimated according to Bonferroni's correction (α_c = 0.05/3).
* Statistically significant for α_c.

quency bands during C1 and C2. The contrasts between C1 and C2 (C2/C1 ratios) were calculated for each stage. They are summarized in Table 2 and presented in subplot B of Fig. 3. For N2, the C2/C1 ratio was slightly superior to 1 (without statistical significance). For N3 and REM, C2/C1 ratios were both significantly inferior to 1.

3.2. Hippocampal sleep spindles

3.2.1. Static properties

For all but one patients (n° 1), sleep spindles were visually observed during N2 and N3 segments. At the detection step of signal processing, 345 potential spindles were extracted and 138 were validated as spindles. Notice that for the patients n° 3 and n° 5, the total number of spindles was only nine. This number is low and, from the point of view of statistical analysis, adding 9 spindles to 129 (patients n° 2, n° 4 and n° 6) only modify the results marginally. Nevertheless, we have kept these data to show the characteristics of the spindles on as many patients as possible. The mean characteristics of these spindles (duration, mean amplitude, first main frequency, second main frequency), computed for each patient, are summarized in Table 3. The related histograms, for all patients, are displayed in subplots A to F of Fig. 4. The 244 main frequencies (1st and 2nd) could be visually split into two bands ranging from 9 to 11.5 Hz (mean: 9.7 Hz) and from 11.5 to 16 Hz (mean: 13.5 Hz) (subplot C of Fig. 4). The percentages inside each band were respectively 42% (103/244) and 58% (141/244). The two-sample Kolmogorov-Smirnov test indicated that the two corresponding data sets were not from the same continuous distribution ($p < 0.001$) that is, they were two distinct sets of frequencies. The repartition of the main frequencies in the two bands is summarized in the first two lines of Table 4. The subplot A of Fig. S2 represents the first main frequency vs. the mean amplitude of the spindles, for the five concerned patients. This subplot showed that there was no obvious correlation between the mean amplitude and the first main frequency of the spindles. For these patients and for all the 106 spindles that exhibit two main frequencies, the subplots A1 and A2 of Fig. S3 represent respectively the second main frequency vs. the first main frequency and the lower main frequency vs. the upper main frequency. When the first main frequency was located within the band 9–11.5 Hz, then the related second main frequency was only located within the band 11.5–16 Hz; the corresponding percentage, for all the frequency pairs, was 30% (32/106). When the first main frequency was located within the band 11.5–16 Hz, then the related second main frequency was mainly located within the band 9–11.5 Hz; the corresponding percentage was 64% (68/106) (subplot A1 of Fig. S3). If we consider now the less restrictive matching between upper and lower main frequencies, then 94% (100/106) of the lower main frequencies were located within the band 9–11.5 Hz when all the upper main frequencies were located within the band 11.5–16 Hz (subplot A2 of Fig. S3). The percentage of spindles that could be modeled by a simple sinusoid with modulated amplitude (single-frequency spindle) was 23% (32/138) (subplot F of Fig. 4 and subplot A of Fig. S4) and are highlighted in the subplot A of Fig. S2. For the three patients (n° 2, 4 and 6) with more than ten spindles, the percentages of single-frequency spindle were respectively 13% (6/47), 16% (3/19) and 33% (21/63).

3.2.2. Dynamic properties

The time–frequency representations of the mean spindle of each patient for five spindle duration intervals (less than 0.6 s, greater than 1.2 s and that range between 0.6 and 0.8 s, 0.8 and 1 s, 1 and 1.2 s) are displayed in Figs. S5–S9. These figures did not exhibit a specific time–frequency signature of the spindles. The time courses of the band-pass filtered spindles, of the associated mobilities and of the mobilities's mean are represented in Fig. 5 and the time courses of the mobilities's mean for each patient are shown in Fig. S10. No particular trend was observed on the mobility except in two cases. First, during the first 200 ms, a subset of curves seemed to start with a main frequency around 10–12 Hz and evolve to a higher frequency. This trend was particularly obvious for patient n° 2 as shown in subplot C of Fig. 5. Nevertheless the mobility of other patients seemed not to follow the same trend, especially patient n° 6 for which the variation of the mobilities's mean was low (subplot E of Fig. S10). Second, at the end of the spindle, some mobility values decreased towards lower frequencies (subplot B of Fig. 5). Therefore, to assess the weight of the beginning and end parts of the spindle in determining the repartition of the first and second main frequencies, we removed successively the first and the last 100 samples of the spindles (i.e. about 195 ms). The updated histograms are represented in subplots G to I (without the first 100 samples) and J to L (without the last 100 samples) of Fig. 4. Furthermore, the new repartitions of the first main frequency vs. the mean amplitude are represented in subplot B (without the first 100 samples) and C (without the last 100 samples) of Fig. S2 and these concerning the second main frequency vs. the first main frequency and the lower main frequency vs. the upper main frequency are respectively displayed in subplots B1 and B2 (without the first 100 samples) and C1 and C2 (without the last 100 samples). The updated percentages of main frequencies inside the bands 9–11.5 Hz and 11.5–16 Hz were indicated in the last four lines of Table 4. The percentage of single-frequency spindles was henceforth 44% (61/138) in the case of removing the first 100 samples (subplot I of Fig. 4 and B of Fig. S4) and 43% (59/138) in the case of removing the last 100 samples (subplot L of Fig. 4 and C of Fig. S4). For patients n° 2, 4 and 6,

Table 3
Summary of number and mean characteristics of sleep spindles.

Patient	Number (%) of spindles	Duration (s)	Mean amplitude (μV)	1st main frequency (Hz)	2nd main frequency (Hz)
2	47 (34%)	0.79 ± 0.20	108.48 ± 20.61	12.40 ± 2.30	11.37 ± 2.02
3	5 (3%)	0.83 ± 0.15	70.93 ± 17.29	12.15 ± 1.98	11.83 ± 2.75
4	19 (14%)	0.81 ± 0.26	97.10 ± 31.13	11.49 ± 1.77	12.52 ± 2.75
5	4 (3%)	0.83 ± 0.27	60.27 ± 9.70	13.13 ± 2.57	10.13 ± 0.97
6	63 (46%)	0.92 ± 0.25	117.03 ± 39.66	12.75 ± 1.14	10.65 ± 1.99

The percentages (%) were related to the total number of spindles ($n = 138$). First main frequency: dominant frequency with the maximal power. Second main frequency: frequency with the maximal power after removing the first main frequency. Notice that the second main frequency was not always present in all spindles.

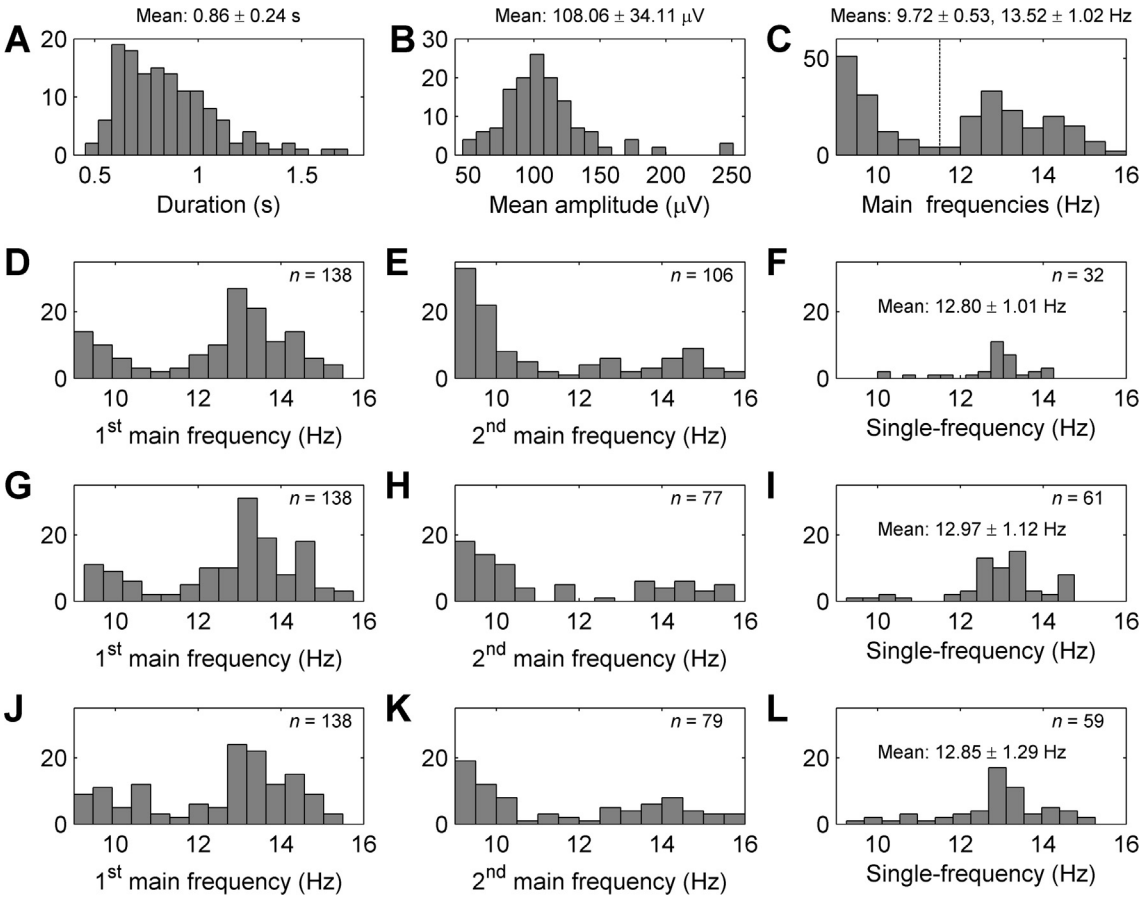

Fig. 4. Histograms of the characteristics of the 138 selected sleep spindles (N2 and N3 segments). (A) duration. (B) mean amplitude. (C), (D), (E) and (F) are frequency characteristics computed on the whole duration of spindles. (C) main frequencies (1st and 2nd); the dotted line indicates the separation in two bands ranging from 9 to 11.5 Hz and from 11.5 to 16 Hz; the indicated means correspond to the values computed for the two bands. (D) first main frequency, i.e. dominant frequency with the maximal power. (E) second main frequency, i.e. frequency with the maximal power after removing the dominant frequency. (F) single-frequency, i.e. dominant frequency in the case of absence of second main frequency. (G), (H) and (I) are frequency characteristics computed on an updated window that start at the beginning of the spindle + 100 samples (≈195 ms) and finish at the end of the spindle. (G) first main frequency, i.e. dominant frequency with the maximal power. (H) second main frequency, i.e. frequency with the maximal power after removing the dominant frequency. (I) single-frequency, i.e. dominant frequency in the case of absence of second main frequency. (J), (K) and (L) are frequency characteristics computed on an updated window that start at the beginning of the spindle and finish at the end of the spindle – 100 samples. (J) first main frequency, i.e. dominant frequency with the maximal power. (K) second main frequency, i.e. frequency with the maximal power after removing the dominant frequency. (L) single-frequency, i.e. dominant frequency in the case of absence of second main frequency.

Table 4
Summary of proportions of sleep spindles in two defined frequency bands.

Analysis epoch	Main frequency set	9–11.5 Hz band	11.5–16 Hz band
The whole spindle	1st main frequency	25% (35/138)	75% (103/138)
The whole spindle	2nd main frequency	64% (68/106)	36% (38/106)
The spindle without the first 100 samples	1st main frequency	22% (30/138)	78% (108/138)
The spindle without the first 100 samples	2nd main frequency	61% (47/77)	39% (30/77)
The spindle without the last 100 samples	1st main frequency	29% (40/138)	71% (98/138)
The spindle without the last 100 samples	2nd main frequency	53% (42/79)	47% (37/79)

The frequency window of analysis could be split up in two bands (9–11.5 and 11.5–16 Hz) according to the main frequencies distribution. The repartition of the main frequencies into these bands was indicated for the whole spindles, for the spindles without the first 100 samples (≈195 ms) and for the spindles without the last 100 samples. First main frequency: dominant frequency with the maximal power. Second main frequency: frequency with the maximal power after removing the first main frequency.

these percentages were respectively 32% (15/47), 32% (6/19) and 57% (36/63) in the former case and 36% (17/47), 26% (5/19) and 54% (34/63) in the latter case.

3.2.3. Validation of the observed trends

The visual analysis of subplots D to L of Fig. 4 seemed to reveal two trends: first, the proportion of first main frequency appeared to be higher in the 11.5–16 Hz band than in the 9–11.5 Hz band (and contrariwise the proportion of second main frequency seemed to be higher in the 9–11.5 Hz band than in the 11.5–16 Hz band); second, the proportion of single-frequency spindles seemed to be higher after removing the first or the last 100 samples. To validate these trends, we performed five unilateral tests of proportions comparison summarized in the first five lines of Table 5. Moreover, to assess whether the suppression of the first or the last 100 samples of the spindles modifies the proportion of main frequencies in the 11.5–16 Hz band (and jointly in the 9–11.5 Hz band), we also performed four bilateral tests of proportions

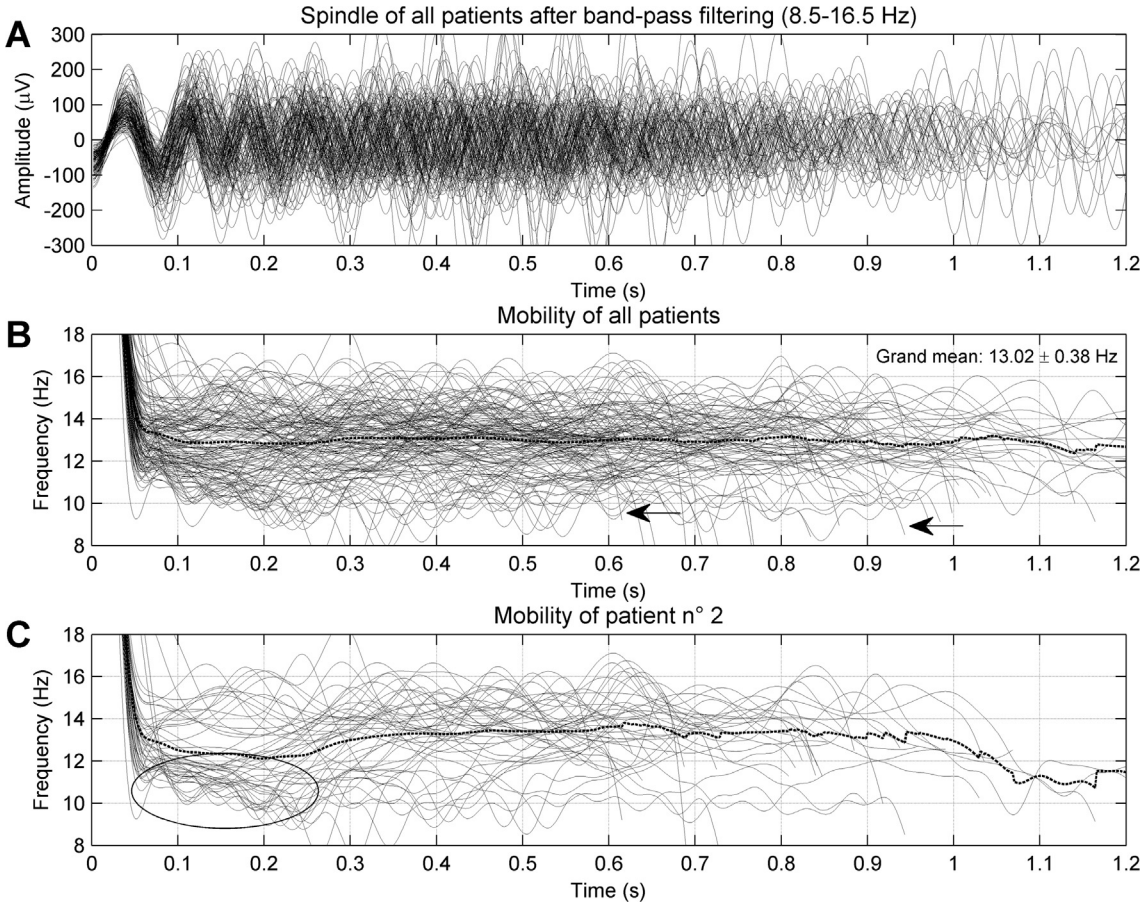

Fig. 5. (A) and (B) Time course of the 138 band-pass filtered sleep spindles (A) and of the corresponding mobility (B). The first 100 ms correspond to the initialization of the algorithm that computes the mobility. The dotted line corresponds to the mean of the mobilities. The grand mean, i.e. the mean of the time course of the means, is computed from 100 ms. The arrows indicate two examples of the decreasing of the mobility at the end of the spindle suggesting that the dominant frequency of some spindles decreased at the end of the transient. (C) Time course of the mobility for the 47 sleep spindles of patient n° 2. The dotted line corresponds to the mean of the mobilities. The ellipse corresponds to a subset of curves that seems to start with a main frequency around 10–12 Hz and evolve to a higher frequency.

Table 5
Summary of proportions comparison tests performed on frequency values of sleep spindles.

H_1 Hypothesis	Proportion difference	Lower limit	Upper limit	P value
P(1st m. f.) > P(2nd m. f.) for band 2 and for whole spindles	0.39	0.24	0.54	<0.001*
P(1st m. f.) > P(2nd m. f.) for band 2 and for spindles without the first 100 samples	0.39	0.24	0.54	<0.001*
P(1st m. f.) > P(2nd m. f.) for band 2 and for spindles without the last 100 samples	0.24	0.08	0.40	<0.001*
P(s.-f. for spindles without the last 100 samples) > P(s. f. for whole spindles)	0.20	0.06	0.34	<0.001*
P(s.-f. for spindles without the first 100 samples) > P(s. f. for whole spindles)	0.21	0.07	0.35	<0.001*
P(1st m. f. for spindles without the first 100 samples) ≠ P(1st m. f. for whole spindles) for band 2	−0.04	−0.18	0.11	0.478
P(2nd m. f. for spindles without the first 100 samples) ≠ P(2nd m. f. for whole spindles) for band 2	−0.03	−0.23	0.17	0.667
P(1st m. f. for spindles without the last 100 samples) ≠ P(1st m. f. for whole spindles) for band 2	0.04	−0.11	0.18	0.499
P(2nd m. f. for spindles without the last 100 samples) ≠ P(2nd m. f. for whole spindles) for band 2	−0.11	−0.31	0.09	0.132

For each test, the H_0 hypothesis is that the indicated proportions in H_1 hypothesis are equal. The value of the proportion difference is presented with lower and upper limits of its confidence interval, estimated according to Bonferroni's correction (α_c = 0.05/9). P(.): proportion. 1st m. f.: first main frequency. 2nd m. f.: second main frequency. s.-f.: single-frequency. Band 2: 11.5–16 Hz band.

* Statistically significant for α_c.

comparison summarized in the four last lines of Table 5. The results of these tests indicated that: (i) the first main frequency of spindles was mainly located in the 11.5–16 Hz band and the second main frequency in the 9–11.5 Hz band, (ii) the proportion of single-frequency spindle increased after removing the first or the last 100 samples (≈195 ms), (iii) removing the first or the last 100 samples did not significantly modify the proportion of the main frequencies in the 9–11.5 Hz and 11.5–16 Hz bands.

4. Discussion

This new simultaneous SEEG-polygraphic study pointed out for the first time the heterogeneity of human hippocampal NREM sleep by clearly distinguishing hippocampal N2 from N3 sleep. We also observed striking dynamic properties of the hippocampal spindles, the 11.5–16 Hz frequency band being mainly dominant, whereas, in some cases, the 9–11.5 Hz frequency band heightened

during the beginning and the end of the transient. Lastly, the power of the hippocampal signal decreased between the first and the second sleep cycle, suggesting a possible homeostatic process within the hippocampus. These results may have some limits because of the restricted number of analyzed patients, the heterogenous quality of sleep across patients (especially in terms stages durations and spindles abundance) and the confounding effect of residual antiepileptic drugs on the various outcomes. These remain common intrinsic limitations of intracerebral studies in humans.

We observed a significant increase of absolute powers for the four frequency bands from N2 to N3 sleep during the first sleep cycle. Hippocampal N3 sleep seems to be characterized by an enhanced electrical activity. Moreover, taking into account the second sleep cycle C2, we observed that the only frequency band differentiating N2 from N3 with sustainability across sleep cycles was the delta band. Similar to cortical N3, the delta component seems to be the most specific criteria defining the hippocampal N3 sleep. The slow-waves might be a common pattern reflecting the information transfer between cortex and hippocampus during N3. In this way, a previous study in humans demonstrated a sequential propagation of slow-waves from cortex to hippocampus during NREM sleep (Nir et al., 2011). Moreover, hippocampal-related mnesic consolidation has been correlated to scalp cortical slow-waves (Molle and Born, 2011), as well as hippocampal slow-waves (2–4 Hz) more recently (Moroni et al., 2014). Therefore, the delta component, specifically individualizing hippocampal N3 sleep in our study, could be one of the substrates of hippocampal-related memory consolidation occurring during N3 sleep.

The sleep spindle is also an essential actor of dialogue between cortical and hippocampal structures (Astori et al., 2013). Actually, most intracerebral studies focused on spindles recorded from cortical regions, especially from frontal and centro-parietal areas, but rarely directly from the hippocampus. Although the presence of hippocampal sleep spindles has been debated for a long time (Malow et al., 1999), recent works have supported the existence of physiological sleep spindles originating from or passing through the hippocampus (Andrillon et al., 2011; Nir et al., 2011; Frauscher et al., 2015). Here we recorded hippocampal spindles that share common features with neocortical spindles but also have specificities. Regardless of the patient, the main characteristics of the spindles seemed to remain close to each other. Nevertheless, for patient n° 3 and n° 5, the very small number of spindles does not allowed them to be used to draw a clear conclusion. Like neocortical spindles, most hippocampal spindles occurred during both N2 and N3 sleep and exhibited two main peaks of frequencies: the first one around 13.5 Hz and the second around 9.7 Hz (subplot C of Fig. 4). The first peak was predominant, which was corroborated both by the spectrum analysis (Fig. 4 and Table 5) and by the time course of mobility (Fig. 5). It was difficult to argue with certainty that the evolution of dominant frequency followed a particular trend. However, we noticed that the beginning of some hippocampal spindles exhibited a close frequency peak around 10–12 Hz which shifts to higher frequencies (subplot C of Fig. 5) and, symmetrically, the dominant frequency of some spindles decreased at the end of the transient. Moreover, the proportion of spindles with a single dominant peak around 13 Hz was almost doubled after removing the initial or final part of the spindles (Figs. 5 and S3). From a signal processing point of view, two interpretations can be suggested to explain these changes in the dominant frequency: (i) a time-varying frequency as an intrinsic property of the hippocampal spindle, or (ii) two combined waves with inverted time course, a first one around 10 Hz whose amplitude decreases at the beginning and increases at the end of the spindle, a second one around 13 Hz whose amplitude increases at the beginning and decreases at the end of the spindle. The first hypothesis is uncertain, because cortical spindles used to show a different time course, which consists in a simple decrease of the dominant frequency at a rate of 0.8 Hz/s (Andrillon et al., 2011). The second hypothesis raises the possibility of two kinds of hippocampal spindles (fast and slow), as observed in cortical areas. In cortical areas, especially in centro-parietal regions, high-powered fast spindles are surrounded by low-powered slow spindles occurring before and after the fast spindle, the timing being orchestrated by slow oscillations (Molle and Born, 2011). This parallel supports the hypothesis that hippocampal spindles might be functionally linked to cortical fast spindles. Recent studies have indeed highlighted the positive correlation between fast spindle activity and hippocampal-related information transfer (Molle and Born, 2011; Astori et al., 2013). The description of human hippocampal spindles appears to be crucial in understanding the mechanisms of memory consolidation during N2 and N3 sleep and further works with such a specific outcome would be helpful.

The REM sleep was characterized by a significant lower absolute power for almost all frequency bands as compared to both N2 and N3 stages (see Fig. 3). In fact, all frequencies were unequally lowered during REM sleep. The absolute power in the delta frequency band was indeed not statistically different between N2 and REM sleep during the first sleep cycle (subplot A of Fig. 3). Therefore hippocampal REM sleep seems to be strongly washed out from all frequencies, the delta band being concerned in a noticeably lesser extent. In a conjectural view, whereas hippocampal activities during NREM sleep seems to gather various and high-powered drives from a wider range of frequencies (including transients), hippocampus during REM sleep might be more likely driven by low-powered slow waves.

Beyond the analysis of hippocampal rhythms according to sleep stages, the effect of sleep cycles on hippocampal activity needs to be taken into account. Although only two full sleep cycles were available for all the patients, we observed a significant decrease of absolute power from the first to the second cycle for N3 and REM stages (see subplot B in Fig. 3). These findings strikingly suggest that part of a homeostatic process within the hippocampus might be similar to that observed within the neocortex (Dijk and Czeisler, 1995). The determination of the homeostatic process in the neocortex was based on the demonstration of a progressive decrease of the delta power across the sleep cycles, and an increase of delta power after a sleep deprivation (Borbély, 1982). We did not carry out a protocol of sleep deprivation. Moreover, the decrease of power from C1 to C2 was independent of the frequency band, but depended on the stages. Further studies will be necessary to specifically address the issue of the homeostatic process in the hippocampus, taking into account the interactions between sleep cycles and sleep stages.

To summarize, this SEEG-polygraphic study provided a new comprehensive overview of the hippocampal activities during sleep by individualizing the hippocampal N2 stage. The time–frequency analysis distinguished indeed N2 from N3 sleep by exhibiting quantitative and even qualitative changes for some frequency bands from one cycle to another. Sleep spindles were also described in the hippocampus during both N2 and N3 sleep. The hippocampal spindles exhibited striking dynamic properties that raises the question of an intrinsic property or an extra-hippocampal drive. Last but not least, the absolute power of hippocampal signal decreased from C1 to C2 for both N3 and REM stages, suggesting a potential homeostatic process within hippocampus. These findings are a new step in defining physiological SEEG patterns in hippocampus during sleep. The knowledge of physiological sleep hippocampal signal might make the epileptologists practicing SEEG better in identifying pathologic patterns. In the research field, this work may contribute to refine future

studies correlating hippocampal electrophysiological activities during sleep and memory processes.

Acknowledgments

The authors would like to thank Lotfi Benkirane (Université de Lorraine) for SEEG data management. No funding.

Conflict of interest: None of the authors have potential conflicts of interest to be disclosed.

Appendix A. Supplementary material

Supplementary data associated with this article can be found, in the online version, at http://dx.doi.org/10.1016/j.clinph.2017.06.248.

References

Andrillon T, Nir Y, Staba RJ, Ferrarelli F, Cirelli C, Tononi G, et al. Sleep spindles in humans: insights from intracranial EEG and unit recordings. J Neurosci 2011;31:17821–34.

Astori S, Wimmer RD, Luthi A. Manipulating sleep spindles–expanding views on sleep, memory, and disease. Trends Neurosci 2013;36:738–48.

Bódizs R, Kántor S, Szabó G, Szûcs A, Erõss L, Halász P. Rhythmic hippocampal slow oscillation characterizes REM sleep in humans. Hippocampus 2001;11:747–53.

Borbély AA. A two process model of sleep regulation. Hum Neurobiol 1982;1:195–204.

Cantero JL, Atienza M, Stickgold R, Kahana MJ, Madsen JR, Kocsis B. Sleep-dependent theta oscillations in the human hippocampus and neocortex. J Neurosci 2003;23:10897–903.

Clemens Z, Weiss B, Szucs A, Eross L, Rásonyi G, Halász P. Phase coupling between rhythmic slow activity and gamma characterizes mesiotemporal rapid-eye-movement sleep in humans. Neuroscience 2009;163:388–96.

Dijk DJ, Czeisler CA. Contribution of the circadian pacemaker and the sleep homeostat to sleep propensity, sleep structure, electroencephalographic slow waves, and sleep spindle activity in humans. J Neurosci 1995;15:3526–38.

Frauscher B, Bernasconi N, Caldairou B, von Ellenrieder N, Bernasconi A, Gotman J, et al. Interictal Hippocampal Spiking Influences the Occurrence of Hippocampal Sleep Spindles. Sleep 2015;38:1927–33.

Genzel L, Kroes MC, Dresler M, Battaglia FP. Light sleep versus slow wave sleep in memory consolidation: a question of global versus local processes? Trends Neurosci 2014;37:10–9.

Hjorth B. The physical significance of time domain descriptors in EEG analysis. Electroencephalogr Clin Neurophysiol 1973;34:321–5.

Iber C. The AASM manual for the scoring of sleep and associated events – rules, terminology and technical specifications. Westchester, IL: American Academy of Sleep Medicine; 2007.

Jadhav SP, Kemere C, German PW, Frank LM. Awake hippocampal sharp-wave ripples support spatial memory. Science 2012;336:1454–8.

Jonas J, Rossion B, Brissart H, Frismand S, Jacques C, Hossu G, et al. Beyond the core face-processing network: Intracerebral stimulation of a face-selective area in the right anterior fusiform gyrus elicits transient prosopagnosia. Cortex 2015;72:140–55.

Kahane P, Landré E, Minotti L, Francione S, Ryvlin P. The Bancaud and Talairach view on the epileptogenic zone: a working hypothesis. Epileptic Disord 2006;8(Suppl 2):S16–26.

Kay SM. Modern spectral estimation. 1988 ed. Pearson Education India; 1988.

Malow BA, Carney PR, Kushwaha R, Bowes RJ. Hippocampal sleep spindles revisited: physiologic or epileptic activity? Clin Neurophysiol 1999;110:687–93.

Molle M, Born J. Slow oscillations orchestrating fast oscillations and memory consolidation. Prog Brain Res 2011;193:93–110.

Moroni F, Nobili L, Curcio G, De Carli F, Fratello F, Marzano C, et al. Sleep in the human hippocampus: a stereo-EEG study. PLoS ONE 2007;2:e867.

Moroni F, Nobili L, De Carli F, Massimini M, Francione S, Marzano C, et al. Slow EEG rhythms and inter-hemispheric synchronization across sleep and wakefulness in the human hippocampus. NeuroImage 2012;60:497–504.

Moroni F, Nobili L, Iaria G, Sartori I, Marzano C, Tempesta D, et al. Hippocampal slow EEG frequencies during NREM sleep are involved in spatial memory consolidation in humans. Hippocampus 2014;24:1157–68.

Nir Y, Staba RJ, Andrillon T, Vyazovskiy VV, Cirelli C, Fried I, et al. Regional slow waves and spindles in human sleep. Neuron 2011;70:153–69.

O'Neill J, Senior TJ, Allen K, Huxter JR, Csicsvari J. Reactivation of experience-dependent cell assembly patterns in the hippocampus. Nat Neurosci 2008;11:209–15.

Peigneux P, Laureys S, Fuchs S, Collette F, Perrin F, Reggers J, et al. Are spatial memories strengthened in the human hippocampus during slow wave sleep? Neuron 2004;44:535–45.

R-Core-Team. R: A language and environment for statistical computing. Vienna, Austria: R Foundation for Statistical Computing; 2013.

Sarasso S, Proserpio P, Pigorini A, Moroni F, Ferrara M, De Gennaro L, et al. Hippocampal sleep spindles preceding neocortical sleep onset in humans. Neuroimage 2014;86:425–32.

Skaggs WE, McNaughton BL, Permenter M, Archibeque M, Vogt J, Amaral DG, et al. EEG sharp waves and sparse ensemble unit activity in the macaque hippocampus. J Neurophysiol 2007;98:898–910.

Staba RJ, Wilson CL, Bragin A, Jhung D, Fried I, Engel Jr J. High-frequency oscillations recorded in human medial temporal lobe during sleep. Ann Neurol 2004;56:108–15.

Urrestarazu E, Chander R, Dubeau F, Gotman J. Interictal high-frequency oscillations (100–500 Hz) in the intracerebral EEG of epileptic patients. Brain 2007;130:2354–66.

Wilson MA, McNaughton BL. Reactivation of hippocampal ensemble memories during sleep. Science 1994;265:676–9.